

Iterative Signal Processing for Integrated Sensing and Communication Systems

Zhiqing Wei, Hanyang Qu, Wangjun Jiang, Kaifeng Han, Huici Wu, Zhiyong Feng

Abstract—Integrated sensing and communication (ISAC), with sensing and communication sharing the same wireless resources and hardware, has the advantages of high spectrum efficiency and low hardware cost, which is regarded as one of the key technologies of the fifth generation advanced (5G-A) and sixth generation (6G) mobile communication systems. ISAC has the potential to be applied in the intelligent applications requiring both communication and high accurate sensing capabilities. The fundamental challenges of ISAC system are the ISAC signal design and ISAC signal processing. However, the existing ISAC signal has low anti-noise capability. And the existing ISAC signal processing algorithms have the disadvantages of quantization errors and high complexity, resulting in large energy consumption. In this paper, phase coding is applied in ISAC signal design to improve the anti-noise performance of ISAC signal. Then, the effect of phase coding method on improving the sensing accuracy is analyzed. In order to improve the sensing accuracy with low-complexity algorithm, the iterative ISAC signal processing methods are proposed. The proposed methods improve the sensing accuracy with low computational complexity, realizing energy efficient ISAC signal processing. Taking the scenarios of short distance and long distance sensing into account, the iterative two-dimensional (2D) fast Fourier transform (FFT) and iterative cyclic cross-correlation (CC) methods are proposed, respectively, realizing high sensing accuracy and low computational complexity. Finally, the feasibility of the proposed ISAC signal processing methods are verified by simulation results.

Index Terms—Integrated Sensing and Communication, Joint Sensing and communication, Iterative Signal Processing, 2D FFT, Cyclic Cross-correlation, Energy Efficiency.

I. INTRODUCTION

A. Background

With the rapid development of mobile communication systems towards 5th-generation-advance (5G-A) and 6th-generation (6G), new intelligent applications and services have emerged, such as machine-type communication (MTC), smart city, and extended reality (XR) [1], which require both communication and sensing capabilities. The separated design of sensing and communication will result in the waste of scarce spectrum resources. Integrated sensing and communication (ISAC), with sensing and communication sharing the same wireless resources and hardware, has the advantages of high spectrum efficiency and low hardware cost [2]. Besides, the performance of sensing and communication will be improved via the collaboration between sensing and communication [3], [4]. With ISAC applied in the intelligent applications in 5G-A and 6G, high data rate communication and high accurate sensing could be achieved [5]. Actually, ITU-T's IMT-2030 has regarded ISAC as one of the key potential technologies in the future mobile communication systems [6].

The fundamental challenges of ISAC system are the ISAC signal design and ISAC signal processing. There are significant differences in the signal structure between communication signal and radar signal due to different application scenarios. The existing ISAC signals are classified into communication centric design and radar centric design [7]. In the perspective of mobile communication systems, the ISAC signal based on Orthogonal Frequency Division Multiplexing (OFDM) attracted wide attention, because OFDM is widely applied in mobile communication systems and has excellent performance in both communication and sensing [8]. Since the transmit power of ISAC signal is relatively low compared with radar signal, the power of echo signal of ISAC signal is low. Hence, the anti-noise performance is crucial for ISAC signal design. Besides, the ISAC signal processing with high sensing accuracy and low computational complexity is essential for ISAC system. In this paper, the ISAC signal with anti-noise performance and the ISAC signal processing with high sensing accuracy and low computational complexity are studied.

B. Related Works

In order to improve the anti-noise capability of ISAC signal, the ISAC signal design schemes based on spread spectrum, linear frequency modulation (LFM), and phase coding, are proposed. Chen *et al.* combined direct spread spectrum technology and OFDM, designing the ISAC signal with anti-noise performance [9]. The ISAC signal combining OFDM and LFM obtains large time-bandwidth product, improving the anti-noise performance of ISAC signal. [10] applied the orthogonal LFM signal as the subcarrier and adopts fractional Fourier transform (FRFT) as the modulation and demodulation method. This scheme effectively reduces bit error rate (BER) in Rayleigh channel. However, the performance of sensing is not improved. Phase coding was applied to ISAC signal design in [11], which improves the correlation of ISAC signals, thereby improving the anti-noise performance of ISAC signals. The ISAC signal combining OFDM and spread spectrum requires large bandwidth, which is difficult for mobile communication systems because of the scarce spectrum resources. The ISAC signal combining OFDM and LFM is not compatible to the current mobile communication systems. The ISAC signal combining OFDM and phase coding effectively improves the anti-noise performance and is compatible to the modern mobile communication systems.

ISAC signals based on phase coding have been studied extensively. The main phase coded sequences include pseudo-random sequences [12]–[14], chaotic sequences [15], complete

complementary codes [16] and Golay sequences [17], [18]. Hu *et al.* applied random sequences to design ISAC signals satisfying the requirements of sensing and communication [12]. The deserialized digital sequence is modulated in the corresponding subcarriers, and the information required for sensing and communication is extracted at the RX. A phase-coded OFDM signal design for a single scattering point target was proposed in [13]. Then, they proposed a high-resolution signal processing algorithm [14]. However, the pseudo-random sequences such as m-sequences and Gold sequences do not have ideal cross-correlation. Moreover, there are a limited number of sequence types. Therefore, some studies have paid much attention on chaotic sequences. Zhao *et al.* designed a phase-coding OFDM signal using chaotic sequences, which has a large time-bandwidth product [15]. They further extracted phase code sequence to improve correlation. Besides, the ISAC signal design using chaotic sequences has high flexibility to support different scenarios [15]. However, chaotic sequences have satisfactory correlation only when there are enough coded bits. Recently, Qi *et al.* proposed the phase coding scheme with complete complementary codes, achieving high data rate and accurate target sensing [16]. [17] compared the phase coded sequences and discovered that Golay sequences restrict the peak to average power ratio (PAPR) of ISAC signal with the increase of the number of subcarriers. [18] applied Reed Muller codes to encode random communication bits into Golay sequences, which not only reduces the PAPR of ISAC signal, but also improves the error detection and correction capability of communication. Considering the coding efficiency, PAPR, bit error rate, etc., the Golay sequences are chosen as the coding sequences in this paper.

Since the structure of ISAC signal is different from traditional radar signal, it is necessary to design the signal processing method suitable to ISAC signal. Sturm *et al.* proposed the two-dimensional fast Fourier transform (2D FFT) method for ISAC signal processing [19]. However, there is quantization error in 2D FFT method. Besides, the maximum detection distance of OFDM signal is limited by the length of cyclic prefix (CP). In order to solve this problem, Wu *et al.* in [20] applies virtual cyclic prefix (VCP) into 2D FFT method to estimate the distance and velocity of target. The signal processing method proposed in [21] improves the anti-noise performance and sensing accuracy of ISAC signal by increasing the number of samplings. However, the quantization error in 2D FFT method is relatively large in the above methods, which will degrade the performance of ISAC signal processing.

The resolution of distance and velocity estimation in 2D FFT method is limited by the number of subcarriers and the number of OFDM symbols. In order to reduce the quantization error, Li *et al.* applied fractional Fourier transform (FRFT) to 2D FFT method, proposing 2D FRFT method. The 2D FRFT method increases the number of the points of Fourier transform, so that the quantization error is reduced and the sensing accuracy is improved [22]. However, the computational complexity in [22] is high. [23] designed 2D FFT method for short distance sensing and correlation method with Golay sequences in the preamble for long distance sensing.

The proposed scheme realizes high accuracy of distance and velocity estimation. Since the duration of the preamble is very short, multiple frames are required to achieve high accuracy of velocity estimation [23]. The super resolution methods such as multiple signal classification (MUSIC) [24] and estimating signal parameter via rotational invariance technique (ESPRIT) [25], [26] methods bring large computational complexity to ISAC systems. Overall, 2D FFT method faces the challenge of large quantization error. FRFT and super resolution methods face the challenge of large overhead and computational complexity. Therefore, the ISAC signal processing method with low complexity and high accuracy is required.

C. Our Contributions

In order to design the ISAC signal with anti-noise capability, considering pilot and data symbols in a typical 5G New Radio (NR) frame, the phase coding is applied in the data symbols. Then, the pilot and phase coded data symbols are jointly applied in target sensing. The iterative ISAC signal processing methods with high accuracy and low complexity are proposed. The sensing distance is limited by the length of CP, so that the scenarios of short distance sensing and long distance sensing are considered. In the scenario of short distance sensing, the delay of the echo signal is smaller than the length of CP. While in the scenario of long distance sensing, the delay of the echo signal is larger than the length of CP. The iterative 2D FFT and iterative Cyclic Cross-correlation (CC) methods are designed for short distance sensing and long distance sensing, respectively. The main contributions of this paper are summarized as follows.

- The Phase Coding-OFDM (PC-OFDM) ISAC signal with the pilot and phase coded data symbols is designed. In long range sensing, phase encoding improves signal correlation and signal to noise ratio (SNR), enhancing the performance of sensing. Then, we analyze the CRLB of distance and velocity estimation.
- The iterative 2D FFT and iterative CC methods are designed for the scenarios of short distance sensing and long distance sensing, respectively, realizing the sensing with low complexity and high accuracy. The estimated value obtained in each iteration compensates the phase of the channel information matrix. With the increase of the number of iterations, the sensing accuracy is improving.

D. Outline of This Paper

The remaining parts of this paper are organized as follows. Section II proposes the PC-OFDM ISAC signal. Section III designs the iterative 2D FFT method for short distance sensing. In Section IV, the iterative CC method is designed for long distance sensing. The simulation results are shown in Section V. Section VI summarizes this paper.

II. ISAC SIGNAL MODEL

The block diagram of the ISAC signal is shown in Fig. 1. At the transmitter (TX), a phase coding module is added to encode the bit stream. Then the phase coded data signal

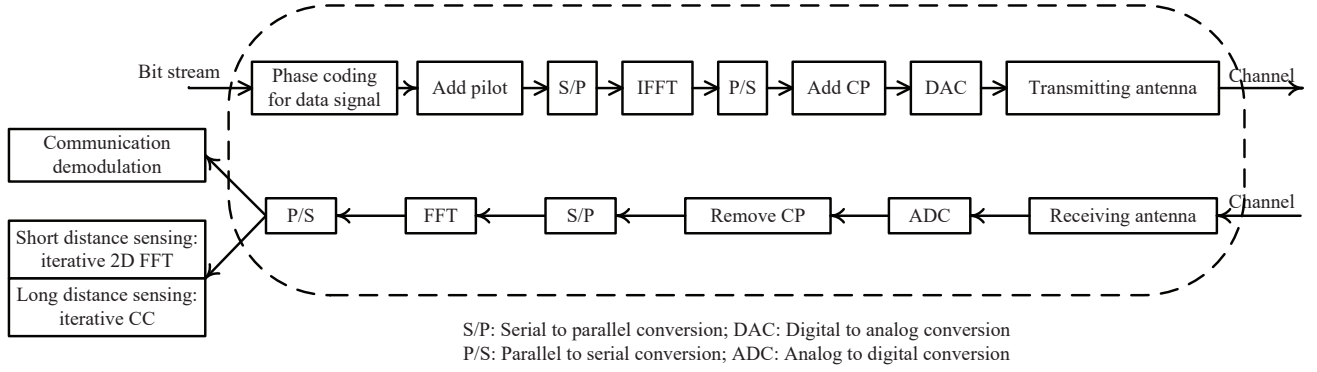


Fig. 1: System model of PC-OFDM ISAC signal.

is combined with the pilot signal for target sensing. At the receiver (RX), the echo signal is sent to the communication demodulation module to obtain the communication information and to the target sensing module to obtain the sensing information of target. In the scenario of short distance sensing, the iterative 2D FFT method is designed. While in the scenario of long distance sensing, the iterative CC method is proposed.

5G NR specifies that the frame of downlink signal includes pilot signal and data signal. In ISAC system, the base station (BS) obtains the distance and velocity of the target by processing the echo of the downlink transmitted signal. The pilot signal is written as follows.

$$s_p(t) = \sum_{m=0}^{M_p-1} \sum_{n=0}^{N_p-1} a_{nm} e^{j2\pi n \Delta f_p t} \text{rect}\left(\frac{t - mT_{sym}}{T_{sym}}\right), \quad (1)$$

where M_p is the number of symbols occupied by the pilot signal, N_p is the number of subcarriers occupied by the pilot signal, a_{nm} is the modulation symbol of the pilot signal modulated on the n -th subcarrier of the m -th OFDM symbol, Δf_p is the interval of subcarrier of the pilot signal, T_{sym} is the duration of OFDM symbol.

The data signal is

$$s_d(t) = \sum_{m=0}^{M_d-1} \sum_{n=0}^{N_d-1} d_{nm} e^{j2\pi n \Delta f t} \text{rect}\left(\frac{t - mT_{sym}}{T_{sym}}\right), \quad (2)$$

where M_d is the number of symbols occupied by the data signal, N_d is the number of subcarriers occupied by the data signal, d_{nm} is the modulation symbol of the data signal modulated on the n -th subcarrier of the m -th OFDM symbol, Δf is the interval of subcarrier of the data signal. Generally, the interval of subcarrier of the pilot signal is the same as that of data signal, namely $\Delta f_p = \Delta f$.

With the combination of pilot and data signals, according to (1) and (2), the transmitted signal is

$$s(t) = s_p(t) + s_d(t). \quad (3)$$

Then, the ISAC signal is obtained by combining the pilot signal and the phase coded data signal. The modulation symbol after phase coding is denoted by d'_{nm} . Hence, the phase coded data signal in the ISAC signal is

$$s_d(t) = \sum_{m=0}^{M_d-1} \sum_{n=0}^{N_d-1} d'_{nm} e^{j2\pi n \Delta f t} \text{rect}\left(\frac{t - mT_{sym}}{T_{sym}}\right). \quad (7)$$

The transmitted signal is reflected by the target. The echo signal is received by the RX. Compared with the transmitted signal, the echo signal includes delay τ and Doppler frequency shift f_d , with expression as follows.

$$r(t) = hs(t - \tau) e^{j2\pi f_d t} = h \times \sum_{m=0}^{M-1} \sum_{n=0}^{N-1} d(n, m) e^{j2\pi n \Delta f (t - \tau)} e^{j2\pi f_d t} \text{rect}\left(\frac{t - \tau - mT_{sym}}{T_{sym}}\right) + \omega(t), \quad (8)$$

where h represents the product of channel attenuation and coefficient of radar cross-section (RCS), $\omega(t)$ is Additive White Gaussian Noise (AWGN), $M = M_p + M_d$ is the number of symbols, N is the number of subcarriers, $d(n, m)$ is the modulation symbol on the n -th subcarrier of the m -th OFDM symbol in the ISAC signal combining the pilot signal and the phase coded data signal.

In long distance sensing, phase coding is applied to enhance the anti-noise performance of ISAC signal. The transmitted ISAC signal $s(t)$ and received ISAC signal $r(t)$ are sampled. The sampling points of them are divided into \tilde{M} groups. The number of sampling points in each group is \tilde{N} [20]. The i -th sampling point of the \tilde{m} -th group of $s(t)$ is denoted by $s_{\tilde{m}}[i]$. The i -th sampling point of the \tilde{m} -th group of $r(t)$ is denoted by $r_{\tilde{m}}[i]$. The VCP with length \tilde{Q} is added [20]. Then, the performance improvement of phase coding on the ISAC signal is demonstrated by deriving the CRLB. The estimation vector θ composed of $\varepsilon = \frac{\tau}{T_b}$ and $v = f_d T_b$ is written as follows.

$$\theta = [\varepsilon, v]^T. \quad (9)$$

The Fisher information matrix is

$$\mathbf{J}(\theta) = \begin{bmatrix} -E \left[\frac{\partial^2 \bar{L}(\theta|r)}{\partial \varepsilon^2} \right] & -E \left[\frac{\partial^2 \bar{L}(\theta|r)}{\partial \varepsilon \partial v} \right] \\ -E \left[\frac{\partial^2 \bar{L}(\theta|r)}{\partial v \partial \varepsilon} \right] & -E \left[\frac{\partial^2 \bar{L}(\theta|r)}{\partial v^2} \right] \end{bmatrix}, \quad (10)$$

where $\bar{L}(\theta|r)$ is the log-likelihood function, r is the echo signal. The log-likelihood function is constructed according

$$-E \left(\frac{\partial^2 \bar{L}(\theta|r)}{\partial \varepsilon^2} \right) = \frac{L}{\sigma^2} \sum_{\tilde{m}=0}^{\tilde{M}-1} \left\{ \frac{1}{3} \sum_{i=0}^{\tilde{Q}-1} \left(\frac{\partial s_{\tilde{m}}[i]}{\partial \varepsilon} \cdot \frac{\partial s_{\tilde{m}}^*[i]}{\partial \varepsilon} \right) + \frac{1}{2} \sum_{i=\tilde{Q}}^{\tilde{N}-1} \left(\frac{\partial s_{\tilde{m}}[i]}{\partial \varepsilon} \cdot \frac{\partial s_{\tilde{m}}^*[i]}{\partial \varepsilon} \right) \right\}, \quad (4)$$

$$-E \left(\frac{\partial^2 \bar{L}(\theta|r)}{\partial v^2} \right) = \frac{L}{\sigma^2} \sum_{\tilde{m}=0}^{\tilde{M}-1} \left\{ \frac{1}{3} \sum_{i=0}^{\tilde{Q}-1} \left(\frac{\partial s_{\tilde{m}}[i]}{\partial v} \cdot \frac{\partial s_{\tilde{m}}^*[i]}{\partial v} \right) + \frac{1}{2} \sum_{i=\tilde{Q}}^{\tilde{N}-1} \left(\frac{\partial s_{\tilde{m}}[i]}{\partial v} \cdot \frac{\partial s_{\tilde{m}}^*[i]}{\partial v} \right) \right\}, \quad (5)$$

$$-E \left(\frac{\partial^2 \bar{L}(\theta|r)}{\partial \varepsilon \partial v} \right) = \frac{L}{4\sigma^2} \sum_{\tilde{m}=0}^{\tilde{M}-1} \left[\begin{array}{l} \frac{2}{3} \sum_{i=0}^{\tilde{Q}-1} \left(\frac{\partial s_{\tilde{m}}[i]}{\partial \varepsilon} \frac{\partial s_{\tilde{m}}^*[i]}{\partial v} + \frac{\partial s_{\tilde{m}}^*[i]}{\partial \varepsilon} \frac{\partial s_{\tilde{m}}[i]}{\partial v} \right) \\ + \sum_{i=\tilde{Q}}^{\tilde{N}-1} \left(\frac{\partial s_{\tilde{m}}[i]}{\partial \varepsilon} \frac{\partial s_{\tilde{m}}^*[i]}{\partial v} + \frac{\partial s_{\tilde{m}}^*[i]}{\partial \varepsilon} \frac{\partial s_{\tilde{m}}[i]}{\partial v} \right) \end{array} \right]. \quad (6)$$

to the samplings of the received echo signal, which is shown as follows.

$$\begin{aligned} \bar{L}(\theta|r) &= \ln \left(\prod_{\tilde{m}=0}^{\tilde{M}-1} \left(\prod_{i=0}^{\tilde{Q}-1} \left(\frac{1}{2\pi \times 3 \frac{\sigma^2}{L}} \right)^{\frac{1}{2}} e^{-\frac{(r_{\tilde{m}}[i] - \tilde{s}_{\tilde{m}})^2}{2 \times 3 \frac{\sigma^2}{L}}} \right. \right. \\ &\quad \cdot \left. \prod_{i=\tilde{Q}}^{\tilde{N}-1} \left(\frac{1}{2\pi \times 2 \frac{\sigma^2}{L}} \right)^{\frac{1}{2}} e^{-\frac{(r_{\tilde{m}}[i] - \tilde{s}_{\tilde{m}})^2}{2 \times 2 \frac{\sigma^2}{L}}} \right) \\ &= \frac{\tilde{Q}\tilde{M}}{2} \ln \frac{2}{3} + \frac{\tilde{N}\tilde{M}}{2} \ln \frac{L}{4\pi\sigma^2} \\ &\quad - \frac{L}{6\sigma^2} \sum_{\tilde{m}=0}^{\tilde{M}-1} \left(\sum_{i=0}^{\tilde{Q}-1} (r_{\tilde{m}}[i] - \tilde{s}_{\tilde{m}}[i]) (r_{\tilde{m}}^*[i] - \tilde{s}_{\tilde{m}}^*[i]) \right. \\ &\quad \left. + \sum_{i=\tilde{Q}}^{\tilde{N}-1} (r_{\tilde{m}}[i] - \tilde{s}_{\tilde{m}}[i]) (r_{\tilde{m}}^*[i] - \tilde{s}_{\tilde{m}}^*[i]) \right), \end{aligned} \quad (11)$$

$$\tilde{s}_{\tilde{m}}[i] = h s_{\tilde{m}}[i - \varepsilon] e^{j2\pi v(\tilde{m}\tilde{N} + i)}, \quad (12)$$

$$L = 10 \log(\tilde{N}), \quad (13)$$

where σ^2 is the power of AWGN, L is the SNR gain obtained by coherent demodulation of the phase coded signal at RX, which is related to the length of the phase code participating in coherent accumulation.

The first derivative and the second derivative of the estimation vector θ are obtained by the log-likelihood function. The elements in Fisher information matrix are given as (4) (5) (6) at the top of this page, where $s_{\tilde{m}}^*[i]$ is the conjugate of $s_{\tilde{m}}[i]$. CRLB is the inverse of Fisher information matrix. The CRLB of ε and v are as follows.

$$\begin{aligned} I_{CRLB,\varepsilon} &= \frac{\mathbf{J}(2,2)}{\mathbf{J}(1,1)\mathbf{J}(2,2) - \mathbf{J}(1,2)\mathbf{J}(2,1)} \\ &= \frac{6}{\pi^2 |h|^2 L \cdot SNR \left(\tilde{N} - \frac{\tilde{Q}}{3} \right) N \left(4 - \left(\frac{\tilde{N}}{\tilde{N}} \right)^2 \right)}, \end{aligned} \quad (14)$$

$$\begin{aligned} I_{CRLB,v} &= \frac{\mathbf{J}(1,1)}{\mathbf{J}(1,1)\mathbf{J}(2,2) - \mathbf{J}(1,2)\mathbf{J}(2,1)} \\ &= \frac{4}{3\pi^2 |h|^2 L \cdot SNR \left(\tilde{N} - \frac{\tilde{Q}}{3} \right) N \tilde{M} (\tilde{M} - 1)}, \end{aligned} \quad (15)$$

where $\mathbf{J}(m,n)$ is the element of m -th row and n -th column in matrix \mathbf{J} , SNR is the SNR of the received echo signal. According to the relation between distance and ε , and the relation between velocity and v , the CRLBs of distance and velocity estimation are derived as follows.

$$I_{CRLB,R} = \frac{3T_b^2 c^2}{2\pi^2 |h|^2 L \cdot SNR} \cdot \frac{1}{\left(\tilde{N} - \frac{\tilde{Q}}{3} \right) N \left(4 - \left(\frac{\tilde{N}}{\tilde{N}} \right)^2 \right)}, \quad (16)$$

$$I_{CRLB,V} = \frac{c^2}{3\pi^2 |h|^2 L \cdot SNR \cdot T_b^2 f_c^2} \cdot \frac{1}{\left(\tilde{N} - \frac{\tilde{Q}}{3} \right) N \tilde{M} (\tilde{M} - 1)}, \quad (17)$$

where T_b is sampling interval, c is the propagation velocity of light, f_c is carrier frequency. It is revealed that CRLB is related to the SNR gain L due to coherent accumulation benefited from phase coding. Hence, the phase coding effectively improves the anti-noise performance of ISAC signal.

III. SHORT DISTANCE SENSING

This section studies the ISAC signal processing algorithm in the scenario of short distance sensing. The pilot and data signals are both applied for target sensing. The 2D FFT method is applied to process the ISAC signal. Besides, the iterative 2D FFT algorithm is designed to achieve the ISAC signal processing with high accuracy and low complexity, which effectively reduces the quantization error caused by 2D FFT method.

A. 2D FFT Method

When receiving the echo signal, the RX applies 2D FFT method to process the echo signal. 2D FFT method was firstly proposed by Strum *et al.*, which has the advantage of low computational complexity. The 2D FFT method proposed in [19] is applied for ISAC signal processing. Since the pilot signal has good correlation and stronger power compared with the data signal, the pilot signal is selected for the first delay estimation. Besides, the pilot signal and data signal are combined for the velocity estimation. Firstly, the echo signal is sampled with the sampling interval T_{sym} in time domain and the sampling interval Δf in frequency domain to obtain the sampling result $d_{Rx}(mM + n)$. According to the samplings of transmitted signal $d_{Tx}(mM + n)$ and received signal $d_{Rx}(mM + n)$, the transmitted symbol matrix \mathbf{T}_τ and received symbol matrix \mathbf{R}_e are constructed. The channel information matrix \mathbf{Y} is

obtained by dividing the received symbol matrix \mathbf{R}_e by the transmitted symbol matrix \mathbf{T}_r element by element. We have $\mathbf{Y} = \mathbf{k}_r \otimes \mathbf{k}_v$ with \otimes representing the Kronecker product. \mathbf{k}_r and \mathbf{k}_v are vectors about time delay and Doppler frequency shift respectively, which are written as follows.

$$\mathbf{k}_r = [1, e^{-j2\pi\Delta f\tau}, \dots, e^{-j2\pi(N_p-1)\Delta f\tau}], \quad (18)$$

$$\mathbf{k}_v = [1, e^{j2\pi T_{sym}f_d}, \dots, e^{j2\pi(M_p+M_d-1)T_{sym}f_d}]. \quad (19)$$

In the next subsection, the ISAC signal combining pilot and phase coded data signal is applied, which improves the sensing performance because of a large number of OFDM symbols and subcarriers.

The peak indexes of the 2D FFT of \mathbf{Y} , denoted by k_1 and l_1 , are obtained, revealing the delay and Doppler frequency shift, so as to obtain the initial estimation of distance and velocity of the target as follows [19].

$$R = \frac{c}{2N_p\Delta f_p}k_1 = \frac{c}{2B}k_1, \quad (20)$$

$$V = \frac{cl_1}{2f_cT_{sym}(M_p + M_d)}, \quad (21)$$

where $B = N_p\Delta f_p$ is the bandwidth of ISAC signal. There are still a large quantization error in 2D FFT method. Thus, the iterative 2D FFT method is designed to improve the sensing accuracy with low complexity.

B. Iterative 2D FFT Method

This section proposes iterative 2D FFT method for the scenario of short distance sensing, reducing the quantization error caused by 2D FFT method. The algorithm is shown in Fig. 2. The channel information matrix is obtained via dividing the transmitted symbol matrix by the received symbol matrix element by element. Then, the first estimation result is obtained by 2D FFT. If the sensing accuracy does not meet the requirement, the phase of the channel information matrix is compensated based on the first estimation result. The second estimation result is obtained based on phase compensation. The above processes are executed iteratively until the sensing accuracy satisfies the requirement.

Take distance estimation as an example. The delay τ is written as

$$\tau = \sum_{i=1}^X \tau_i, \quad (22)$$

where τ_i is the estimated delay in i -th iteration, X is the number of iterations. With the initial delay estimation, the τ_i is as follows.

$$\tau_i = \begin{cases} \frac{k_i - 0.5}{\Delta f_p N_p N_d^{i-1}}, & i < X \\ \frac{k_i}{\Delta f_p N_p N_d^{i-1}}, & i = X \end{cases}. \quad (23)$$

In (23), k_i is the peak index obtained in i -th iteration. In Section III-A, the peak index k_1 is obtained. Thus τ_1 is derived via (23). The m -th column vector in channel information

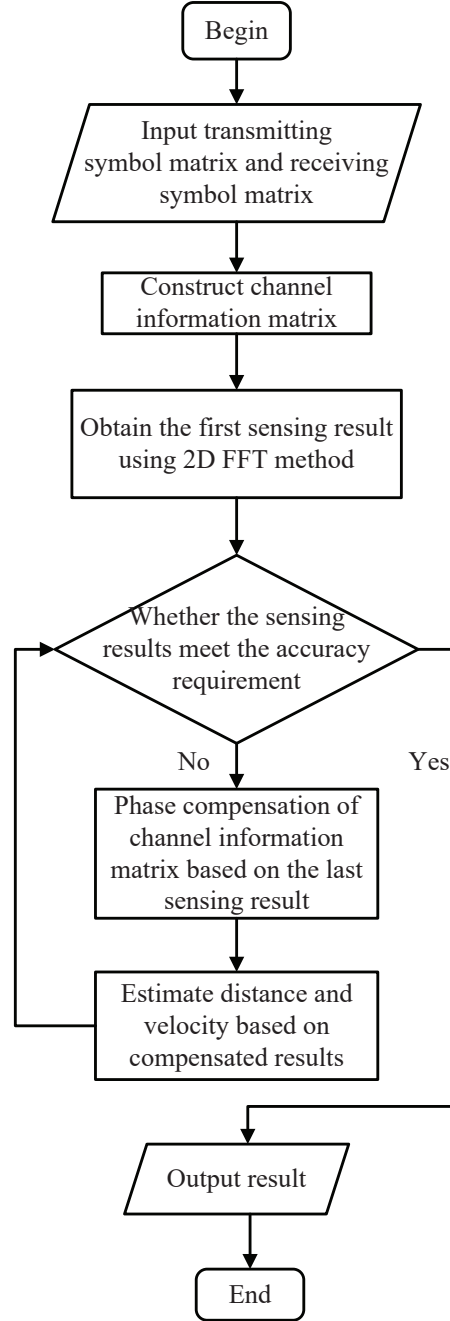


Fig. 2: Iterative 2D FFT method.

matrix \mathbf{Y} is written as (24). The phase compensation of the delay term of m -th column vector in \mathbf{Y} is carried out according to the τ_1 obtained in the first iteration, yielding \mathbf{k}'_{rm} as shown in (25). The IDFT of \mathbf{k}'_{rm} is calculated. By searching the peak of IDFT of \mathbf{k}'_{rm} , the peak index is obtained to estimate the distance of target. The column vector \mathbf{k}_{rm} comes from the data signal, since there are more subcarriers in data signal compared with the pilot signal.

$$\mathbf{k}_{rm} = [1, e^{-j2\pi\Delta f\tau}, \dots, e^{-j2\pi(N_d-1)\Delta f\tau}]^T. \quad (24)$$

$$\mathbf{k}'_{rm} = \mathbf{k}_{rm} \odot \left[1, e^{j2\pi\Delta f\tau_1}, \dots, e^{j2\pi(N_d-1)\Delta f\tau_1} \right]^T, \quad (25)$$

where \odot is the hadamard product.

The IDFT of \mathbf{k}'_{rm} is calculated as follows.

$$\begin{aligned} \mathbf{r}(\bar{k}_d) &= \frac{1}{N_d} \sum_{n=0}^{N_d-1} e^{-j2\pi n\Delta f(\tau-\tau_1)} e^{j2\pi n \frac{\bar{k}_d}{N_p N_d}} \\ &= \frac{1}{N_d} \sum_{n=0}^{N_d-1} e^{-j2\pi n\Delta f\tau_2} e^{j2\pi n \frac{\bar{k}_d}{N_p N_d}} \\ &= \frac{1}{N_d} \sum_{n=0}^{N_d-1} e^{j2\pi n \left(\frac{\bar{k}_d}{N_p N_d} - \Delta f\tau_2 \right)}, \end{aligned} \quad (26)$$

where $\bar{k}_d = 0, 1, \dots, N_d - 1$, $\mathbf{r}(\bar{k}_d)$ is the \bar{k}_d -th element of the IDFT of \mathbf{k}'_{rm} . When there are only two iterations, we have $\tau - \tau_1 = \tau_2$.

Denoting $\Delta\tau = \frac{\bar{k}_d}{N_p N_d} - \Delta f\tau_2$, (26) is transformed as follows.

$$\begin{aligned} \mathbf{r}(\Delta\tau) &= \frac{1}{N_d} \sum_{n=0}^{N_d-1} e^{j2\pi n\Delta\tau} \\ &= \frac{1}{N_d} \frac{1 - e^{j2\pi\Delta\tau N_d}}{1 - e^{j2\pi\Delta\tau}} \\ &= \frac{1}{N_d} \frac{e^{-j\pi\Delta\tau N_d} - e^{j\pi\Delta\tau N_d}}{e^{-j\pi\Delta\tau} - e^{j\pi\Delta\tau}} \\ &= \frac{1}{N_d} \frac{\sin(\pi\Delta\tau N_d)}{\sin(\pi\Delta\tau)} e^{j\pi\Delta\tau(N_d-1)} \\ &\approx \text{sinc}(\pi\Delta\tau N_d) e^{j\pi\Delta\tau(N_d-1)}. \end{aligned} \quad (27)$$

In terms of $\text{sinc}(\pi\Delta\tau N_d)$ and $\exp(j\pi\Delta\tau(N_d-1))$ in (27), when $\Delta\tau = 0$, both of them are maximum. Therefore, when $\Delta\tau = 0$, $\mathbf{r}(\bar{k}_d)$ is maximum. Searching the peak of $\mathbf{r}(\bar{k}_d)$, the peak index k_2 is obtained, which satisfies the following equation.

$$\Delta\tau = \frac{k_2}{N_p N_d} - \Delta f\tau_2 = 0. \quad (28)$$

Solving (28), $\tau_2 = \frac{k_2}{\Delta f N_p N_d}$ is obtained. With two iterations, the distance of the target is derived as follows.

$$R = \frac{c}{2} (\tau_1 + \tau_2) = \frac{c}{2\Delta f} \frac{k_1 - \frac{1}{2} + \frac{k_2}{N_p}}{N_d} \quad (29)$$

With X iterations, the accuracy of distance estimation is enhanced. The iteration process is shown in the Fig. 3. Compared with the distance estimation of 2D FFT method, the accuracy of distance estimation with X iterations is

$$\Delta R = \frac{c}{2\Delta f} \cdot \frac{1}{N_p N_d^{X-1}}. \quad (30)$$

Similarly, the above iterative 2D FFT method is applied in velocity estimation. With two iterations, Doppler frequency shift is $f_d = f_{d1} + f_{d2}$, where f_{di} is the estimated Doppler frequency shift in the i -th iteration. When estimating velocity in the first iteration, the peak index obtained by 2D FFT

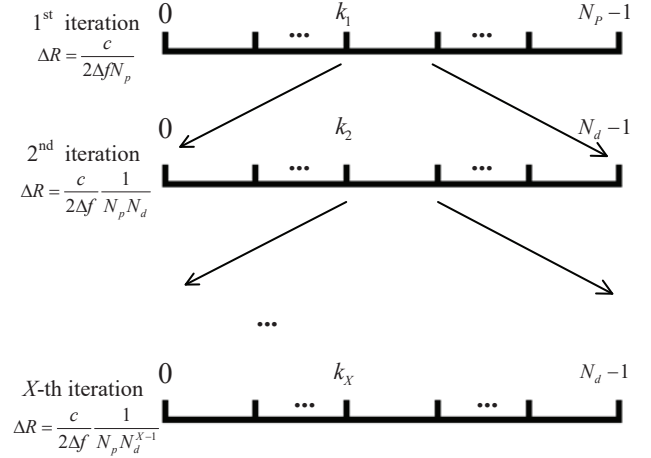


Fig. 3: The iterations of distance estimation.

method is recorded as l_1 , as shown in Section III-A. Phase compensation is performed for each element of the channel information matrix \mathbf{Y} according to the peak index l_1 in the first iteration. Similar to (25), the n -th row of \mathbf{Y} after phase compensation is recorded as \mathbf{k}'_{vn} . The DFT of \mathbf{k}'_{vn} is calculated as follows.

$$\begin{aligned} \mathbf{r}(\bar{l}_d) &= \frac{1}{M_p + M_d} \times \\ &\sum_{m=0}^{M_p+M_d-1} e^{j2\pi m T_{sym}(f_d - f_{d1})} e^{-j2\pi m \frac{\bar{l}_d}{(M_p+M_d)^2}} \\ &= \frac{1}{M_p + M_d} \sum_{m=0}^{M_p+M_d-1} e^{j2\pi m \left(T_{sym} f_{d2} - \frac{\bar{l}_d}{(M_p+M_d)^2} \right)}, \end{aligned} \quad (31)$$

where $\bar{l}_d = 0, 1, \dots, M_p + M_d - 1$, $\mathbf{r}(\bar{l}_d)$ is the \bar{l}_d -th element of the DFT of \mathbf{k}'_{vn} . Searching the peak of $\mathbf{r}(\bar{l}_d)$, the peak index l_2 is obtained. The estimated velocity with two iterations is

$$V = \frac{c}{2f_c T_{sym}} \left(\frac{l_1 - 0.5 + \frac{l_2}{M_p + M_d}}{M_p + M_d} \right). \quad (32)$$

Compared with the velocity estimation of 2D FFT method, the accuracy of velocity estimation with X iterations is enhanced, which is as follows.

$$\Delta V = \frac{c}{2f_c T_{sym} (M_p + M_d)^X}. \quad (33)$$

IV. LONG DISTANCE SENSING

In the scenario of long distance sensing, the CC algorithm is applied to overcome the limitation of CP length on the sensing distance. The concept of VCP is firstly proposed in [20], [27] to realize long distance sensing. [21] proposed another scheme for long distance sensing, where the CC algorithm and maximum likelihood (ML) algorithm are combined to construct the channel information matrix. Then, the CC algorithm is used to estimate the distance and the 2D FFT method is used to estimate the velocity. By increasing the number of samplings, the CC algorithm improves the accuracy of distance estimation. However, the improvement of the accuracy of velocity

estimation is not significant. In order to improve the accuracy of velocity estimation, we have proposed an iterative ISAC signal processing method in Section III-B. In the scenario of long distance sensing, the ISAC signal combining pilot signal and phase coded data signal is applied, which is processed by the iterative CC algorithm. In the scenario of long distance sensing, the SNR of echo signal is low, so that the phase coding improves the anti-noise performance of ISAC signal.

A. The CC Method with VCP and ML

The transmitted ISAC signal $s(t)$ is sampled with the sampling interval T_b , where $T_b = \frac{T_{sym}}{N'}$ and N' is the number of samplings within an OFDM symbol. After removing the CP, the sampling of transmitted signal is obtained. The sampling points are divided into \tilde{M} groups. The number of sampling points in each group is \tilde{N} . The received signal is sampled with the same sampling interval T_b . Similarly, the sampling points are divided into \tilde{M} groups. And the number of sampling points in each group is \tilde{N} [20]. The VCP is added, whose length is \tilde{Q} [20]. VCP is the last \tilde{Q} sampling points in a group, which are added to the first \tilde{Q} sampling points of this group. The i -th sampling point in the \tilde{m} -th group is shown as follows.

$$r_{\tilde{m}}[i] = h s_{\tilde{m}}[i - \varepsilon] e^{j2\pi v(\tilde{m}\tilde{N} + i)} + \omega_{\tilde{m}}[i] + I_{\tilde{m}}[i], \quad (34)$$

where $\varepsilon = \left\lfloor \frac{\tau}{T_b} \right\rfloor$, $I_{\tilde{m}}[i]$ is inter block interference due to VCP and follows Gaussian distribution [20], as shown in (35). Due to the addition of VCP, $\omega_{\tilde{m}}[i]$ follows Gaussian distribution [20], as shown in (36).

$$I_{\tilde{m}}[i] \sim N(0, \sigma^2). \quad (35)$$

$$\omega_{\tilde{m}}[i] \sim \begin{cases} N(0, 2\sigma^2), & 0 \leq i < \tilde{Q} \\ N(0, \sigma^2), & \tilde{Q} \leq i < \tilde{N} \end{cases}, \quad (36)$$

The correlation function $\rho(p)$ is constructed as follows by calculating the correlation between received and transmitted signals [21].

$$\rho(p) = \sum_{i=0}^{\tilde{N}-1} r_{\tilde{m}}[i] s_{\tilde{m}}^*[i - p]. \quad (37)$$

$\rho(p)$ is maximum when $p = \varepsilon$. Searching the peak index $p = \varepsilon$, the delay τ is derived by solving the equation $\varepsilon = \frac{\tau}{T_b}$. Then, the distance of target is estimated.

$s_{\tilde{m}}[i]$ is shifted by ε samplings, yielding the shifted sequence $s_{\tilde{m}}[i - \varepsilon]$. The correlation function $\eta(p, \tilde{m})$ of $s_{\tilde{m}}[i - \varepsilon]$ and the original sequence $s_{\tilde{m}}[i]$ is constructed as follows.

$$\eta(p, \tilde{m}) = \sum_{i=0}^{\tilde{N}-1} s_{\tilde{m}}[i - \varepsilon] s_{\tilde{m}}^*[i - p]. \quad (38)$$

When calculating the correlation function $\eta(p, \tilde{m})$, the received signal is coherently accumulated, increasing the SNR of the received echo signal by $10 \log(\tilde{N})$ times, which improves the anti-noise ability of the ISAC signal [28]. According to

the relation between $r_{\tilde{m}}[i]$ and $s_{\tilde{m}}[i]$ in (34), the ML of ε and v is

$$\begin{aligned} \arg_{ML}(\varepsilon, v) &= \sum_{\tilde{m}=0}^{\tilde{M}-1} \sum_{i=0}^{\tilde{N}-1} \left| \rho(p) - h e^{j2\pi v \tilde{m} \tilde{N}} \eta(p, \tilde{m}) \right|^2 \\ &= \underbrace{\sum_{\tilde{m}=0}^{\tilde{M}-1} \sum_{i=0}^{\tilde{N}-1} |\rho(p)|^2}_{(a)} + \underbrace{\sum_{\tilde{m}=0}^{\tilde{M}-1} \sum_{i=0}^{\tilde{N}-1} |h \eta(p, \tilde{m})|^2}_{(b)} \\ &\quad - 2 \operatorname{Re} \left(\sum_{\tilde{m}=0}^{\tilde{M}-1} \sum_{i=0}^{\tilde{N}-1} \rho(p) \left(h e^{j2\pi v \tilde{m} \tilde{N}} \eta(p, \tilde{m}) \right)^* \right). \end{aligned} \quad (39)$$

The terms (a) and (b) in (39) have nothing to do with ε and v , which do not affect the result of $\arg_{ML}(\varepsilon, v)$. When $\arg_{ML}(\varepsilon, v)$ is minimum, (40) needs to take the maximum value. Therefore, the ML estimation of velocity is transformed into the maximization of $\mu(p, \tilde{m})$ [21].

$$\mu(p, \tilde{m}) = \sum_{\tilde{m}=0}^{\tilde{M}-1} \sum_{i=0}^{\tilde{N}-1} \left| \rho(p) \eta^*(\varepsilon, \tilde{m}) e^{-j2\pi v \tilde{m} \tilde{N}} \right|. \quad (40)$$

When $p = \varepsilon \triangleq p_0$, $\eta^*(\varepsilon, \tilde{m})$ is maximum, which is denoted by η_0 . The p_0 is also the peak index of the correlation function $\rho(p)$ in (37). Similar to [21], letting $v = \frac{l}{M\tilde{N}}$, $l = 0, 1, \dots, \tilde{M} - 1$, (40) is transformed into the following form.

$$\mu(p_0, \tilde{m}) = \eta_0 \left| \sum_{\tilde{m}=0}^{\tilde{M}-1} \rho(p_0) \exp\left(-j2\pi \frac{\tilde{m}l}{\tilde{M}}\right) \right|. \quad (41)$$

The searching of the maximum value of $\mu(p_0, \tilde{m})$ respective to l is regarded as the searching the peak index of the DFT of $\rho(p_0)$. The solution of maximization of $\mu(p_0, \tilde{m})$ is denoted by $l = l_0$. When $\mu(p_0, \tilde{m})$ is maximum, we have (42) with the expansion of (41), and we have (43).

$$\exp(j2\pi v \tilde{m} \tilde{N}) \exp\left(-j2\pi \frac{\tilde{m}l_0}{\tilde{M}}\right) = 1. \quad (42)$$

$$\varepsilon = p_0. \quad (43)$$

Solving the equation (42), the v is obtained as follows.

$$v = \frac{l_0}{\tilde{M}\tilde{N}}. \quad (44)$$

According to (43) and (44), the distance and velocity of target are calculated, respectively.

$$R = \frac{cT_b}{2} p_0, \quad (45)$$

$$V = \frac{c}{2f_c T_b \tilde{M} \tilde{N}} l_0. \quad (46)$$

Then, we have the accuracy of distance and velocity estimation as follows.

$$\Delta R = \frac{cT_b}{2} = \frac{cT_{sym}}{2N'} = \frac{c}{2B} \frac{N}{N'}, \quad (47)$$

$$\Delta V = \frac{c}{2f_c \tilde{N} \tilde{M} T_b} = \frac{c}{2f_c \tilde{M} T_{sym} \tilde{N}} \frac{N'}{N}. \quad (48)$$

B. The Iterative CC Method

According to the algorithm mentioned in Section III-B, the accuracy of distance estimation is improved by increasing the number of sampling points in each OFDM symbol. However, in (48), the product of \tilde{M} and \tilde{N} is N' , so that we have $\Delta V = \frac{c}{2f_c T_{sym}}$, which implies that reducing the sampling interval does not improve the accuracy of velocity estimation. In this subsection, an iterative CC method is proposed to improve the accuracy of velocity estimation. In the first iteration, the velocity is estimated by the CC method. Then, the channel information matrix undergoes phase compensation using the estimated velocity, narrowing the interval of the velocity estimation. The above operations are executed iteratively to obtain a satisfactory accuracy of velocity estimation.

With $p = p_0$ and substituting (37) into (41), we have

$$\mu(p_0, \tilde{m}) = \sum_{\tilde{m}=0}^{\tilde{M}-1} \eta_0 \exp(j2\pi v \tilde{m} \tilde{N}) \exp(-j2\pi \frac{\tilde{m} l}{\tilde{M}}). \quad (49)$$

The vector for velocity estimation in the first iteration is

$$\mathbf{a} = [A_0, \dots, A_{\tilde{m}} e^{j2\pi v \tilde{m} \tilde{N}}, \dots, A_{\tilde{M}-1} e^{j2\pi v (\tilde{M}-1) \tilde{N}}], \quad (50)$$

$$v = v_0 + v_1 + \dots + v_{X-1},$$

where v_0, v_1, \dots, v_{X-1} are the estimated values of v in each iteration, and $A_{\tilde{m}}$ is

$$A_{\tilde{m}} = h \sum_{i=0}^{\tilde{N}-1} s_{\tilde{m}} [i - \varepsilon] s_{\tilde{m}}^* [i - p], \tilde{m} = 0, 1, \dots, \tilde{M} - 1. \quad (51)$$

According to Section III-B, With $l = l_0$, the l -th element of the DFT of \mathbf{a} is maximum. Hence, $l = l_0$ is the peak index in the first iteration. The v_0 in the first iteration is

$$v_0 = \frac{l_0 - \frac{1}{2}}{\tilde{M} \tilde{N}}. \quad (52)$$

With (52), \mathbf{a} undergoes phase compensation, yielding \mathbf{a}' .

$$\mathbf{a}' = \mathbf{a} \odot [1, e^{-j2\pi v_0 \tilde{N}}, \dots, e^{-j2\pi v_0 (\tilde{M}-1) \tilde{N}}]. \quad (53)$$

Then, the second iteration starts, the DFT of \mathbf{a}' is calculated. By searching the maximum value of the DFT of \mathbf{a}' , the peak index $l = l_1$ is obtained. With $l = l_1$, the v_1 is estimated in the second iteration.

$$v_1 = \frac{l_1 - \frac{1}{2}}{\tilde{M}^2 \tilde{N}}. \quad (54)$$

With two iterations, the estimated velocity is expressed as

$$V = \frac{c}{2f_c T_b} \frac{l_0 - \frac{1}{2} + \frac{l_1}{\tilde{M}}}{\tilde{M} \tilde{N}}. \quad (55)$$

With X iterations, the velocity estimation is recorded as V and the accuracy of velocity estimation is ΔV , which is improved compared with CC method.

$$V = \frac{c}{2f_c \tilde{N} T_b} \cdot \left(\sum_{\alpha=0}^{X-2} \frac{l_{\alpha} - 0.5}{\tilde{M}^{\alpha+1}} + \frac{l_{X-1}}{\tilde{M}^X} \right), \quad (56)$$

$$\Delta V = \frac{c}{2f_c \tilde{N} T_b \tilde{M}^X}. \quad (57)$$

When the channel information matrix is obtained, the 2D FFT method calculates M times of N -point IDFT and N times of M -point DFT to estimate the distance and velocity of the target, respectively. Therefore, the computational complexity of 2D FFT algorithm is $O(M^2 + N^2)$. The CC algorithm divides the samplings of transmitted signal and received signal into \tilde{M} groups, with \tilde{N} sampling points in each group. The correlation function of a group of samplings of the transmitted signal and the received signal is calculated, and then the M -point DFT is calculated. Therefore, the computational complexity of CC algorithm is $O(\tilde{M}^2 + \tilde{N}^2)$. Supposing that the iterative 2D FFT method has X iterations, there are M times of N -point IDFT and N times of M -point DFT in each iteration. Therefore, the computational complexity of the iterative 2D FFT method is $O(X * (M^2 + N^2))$. When sensing accuracy of the method in [22] is the same to iterative 2D FFT method, the computational complexity of the method in [22] is $O((M^2 + N^2)^X)$, which is higher than the iterative 2D FFT method proposed in this paper.

V. SIMULATION RESULTS AND ANALYSIS

In this section, the performance of ISAC signal and the performance of iterative signal processing algorithms are verified. The main parameters in Subsections B and C are shown in Table I.

TABLE I: Parameters of ISAC signal

Parameters	Values
Interval of subcarrier	15 kHz
Carrier frequency	24 GHz
Number of subcarriers	256
Numbers of symbols	14
Sampling interval	0.13 μ s

A. Ambiguity Function

Fig. 4 illustrates the ambiguity function (AF) of the ISAC signal combining pilot and data symbols using 32 bit Golay sequence in phase coding. Fig. 5 shows the AF of ISAC signal without phase coding. The number of subcarriers of ISAC signal is 32. The subcarrier interval is set to 15 kHz. The number of OFDM symbols is 10. Comparing Fig. 4 and Fig. 5, it is discovered that the ISAC signal encoded with Golay sequence has a pushpin AF, while the AF of the ISAC signal without phase coding has a triangular envelope. The sidelobe attenuation of the AF of the ISAC signal without phase coding is slower than the AF of the ISAC signal with phase coding. Therefore, phase coding effectively improves the sensing performance of ISAC signal.

B. Short range sensing

Two targets are detected in the scenario of short range sensing to verify the performance improvement of iterative 2D FFT algorithm in Section III. The distance of the two targets is

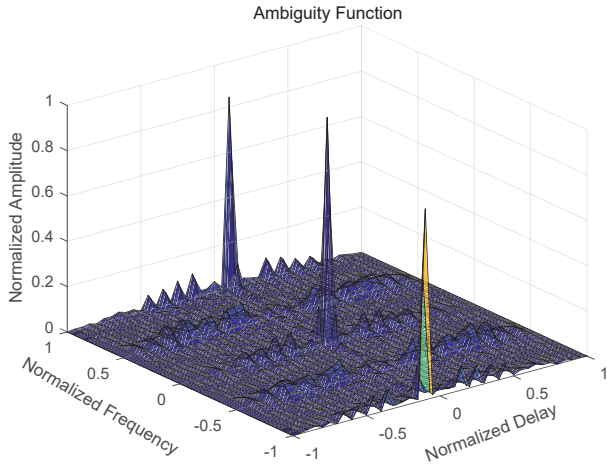


Fig. 4: AF of ISAC signal with phase coding using Golay sequence.

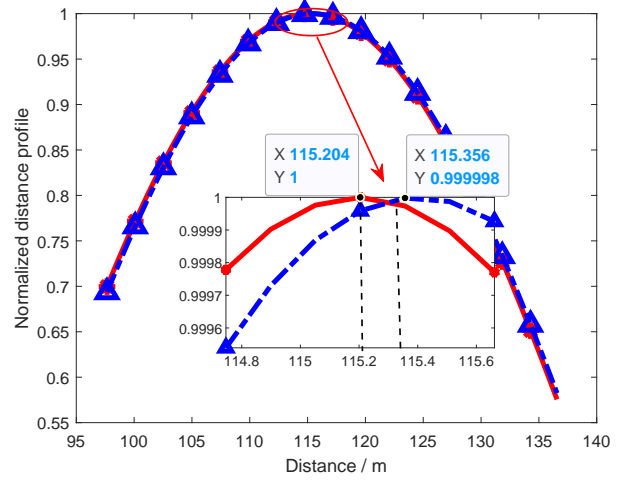


Fig. 6: Distance estimation performance of proposed ISAC signal processing method in short distance sensing.

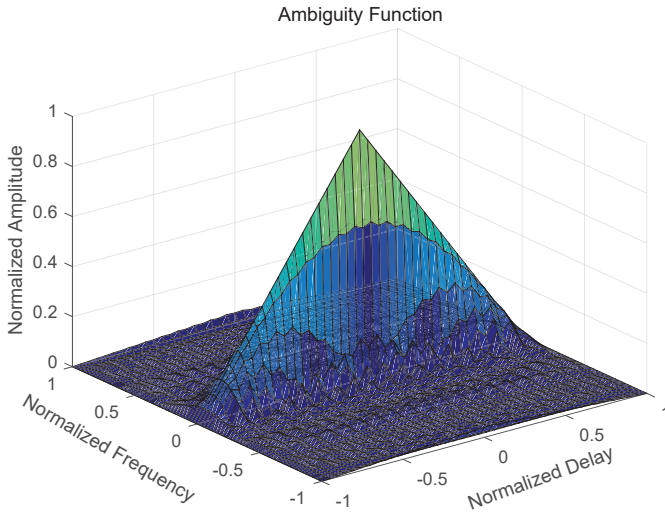


Fig. 5: AF of ISAC signal without phase coding.

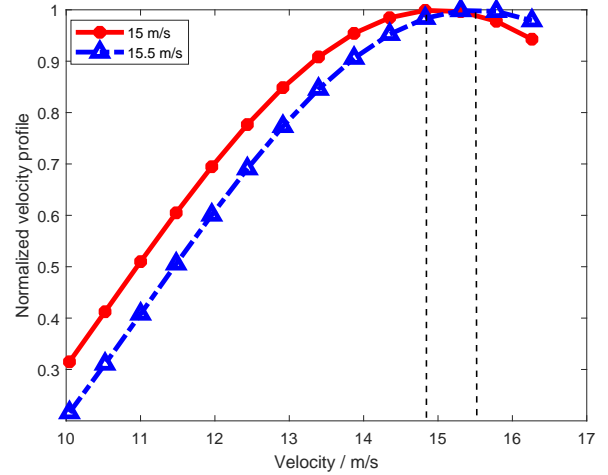


Fig. 7: Velocity estimation performance of proposed ISAC signal processing method in short distance sensing.

115.2 m and 115.4 m, respectively, and the velocity of the two targets is 15 m/s and 15.5 m/s, respectively. Using the iterative 2D FFT algorithm proposed in Section III, the sensing results are shown in Fig. 6 and Fig. 7. It is revealed that the error of distance and velocity estimation is reduced to 0.037 % and 1.2 %, respectively.

In the iterative 2D FFT algorithm, the number of iterations is set as 2. The Root Mean Square Errors (RMSEs) of the estimation of distance and velocity are shown in Fig. 8 and Fig. 9, respectively. With low SNR, the sensing performance of the two algorithms is similar. With the increase of SNR, the RMSE of iterative 2D FFT algorithm is lower than that of 2D FFT algorithm and the gap between them is increasing. Simulation results verified that the proposed iterative 2D FFT algorithm has higher accuracy and effectively overcomes the quantization error of 2D FFT algorithm. It is revealed from the Fig. 8 and Fig. 9 that RMSE first decreases with the increase of SNR, and finally converges to a constant value. This is due to the fact that the estimated values of distance and velocity are related to the

peak indexes at each iteration. However, these peak indexes take integer, so that there is an error between the estimated value and the real value, which is called quantization error. With the increase of the number of iterations, the quantization error decreases. With the increase of SNR, the estimated values of distance and velocity will become more and more accurate and gradually approach the real value. Therefore, RMSE will decrease with the increase of SNR. When the SNR increases to a threshold, the impact of noise on the estimated value is small and can be ignored. Meanwhile, RMSE no longer decreases with the increase of SNR since it is mainly resulted from quantization error.

C. Long range sensing

The performance of ISAC signal processing method in the scenario of long distance sensing is verified in this subsection. According to the simulation parameters in Table I, the target with velocity of 25 m/s and distance of 600 m is detected. The

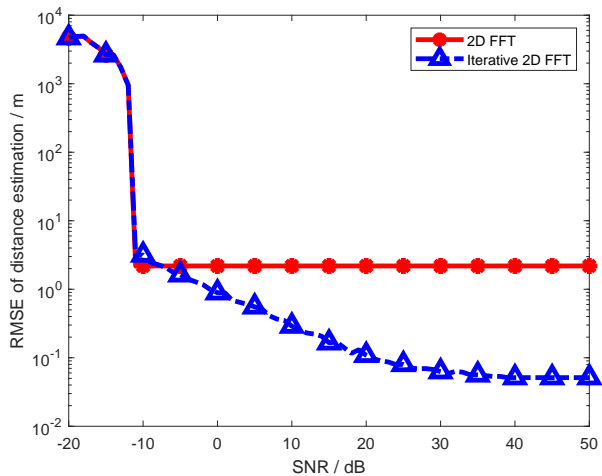


Fig. 8: Distance estimation performance of 2D FFT and iterative 2D FFT methods.

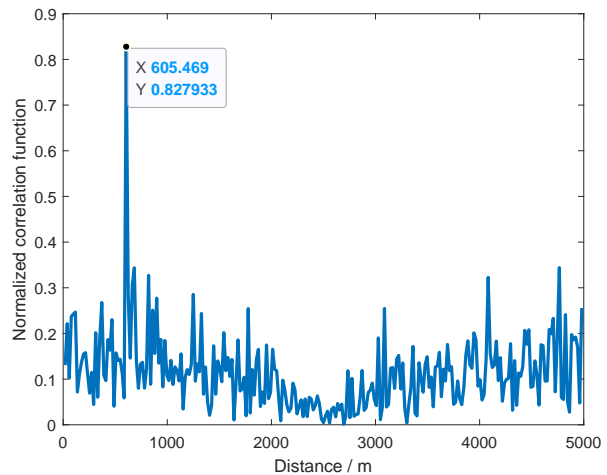


Fig. 10: Distance estimation in the scenario of long distance sensing.

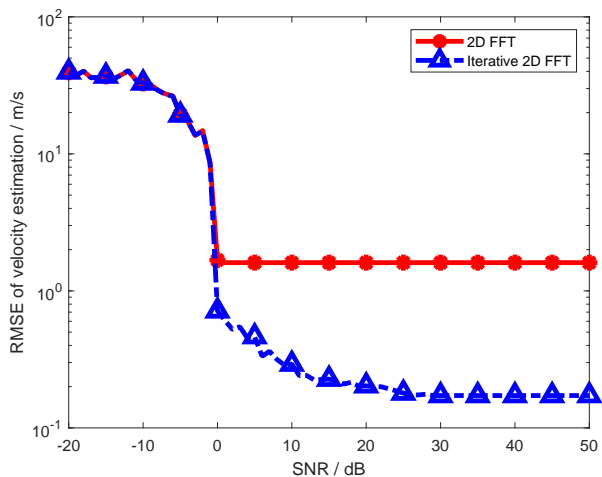


Fig. 9: Velocity estimation performance of 2D FFT and iterative 2D FFT methods.

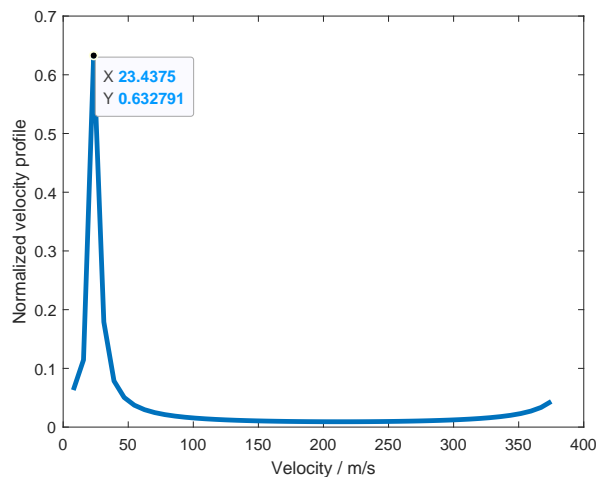


Fig. 11: Velocity estimation in the scenario of long distance sensing.

sensing results of distance and velocity using the iterative CC algorithm are shown in Fig. 10 and Fig. 11. The estimated distance and velocity of target are 605.5 m and 23.44 m/s, respectively, with errors of 0.84 % and 6.24 %, respectively. It is revealed that the iterative CC algorithm correctly estimates the sensing information.

When 32-bit Golay sequence is applied to phase encode the ISAC signal, the RMSE and CRLB of distance and velocity estimation are shown in Fig. 12 and Fig. 13, respectively. It is revealed that the ISAC signal with phase coding has better anti-noise performance, yielding a lower CRLB compared with the ISAC signal without phase coding.

With the parameters in Table I, the velocity accuracy is 7.8125 m/s without iteration according to (48), and the velocity accuracy of the iterative CC algorithm is improved to 0.16 m/s with two iterations according to (57). As shown in Fig. 14, the velocity of the two targets is 25 m/s and 25.16 m/s, respectively. The CC algorithm cannot distinguish the two

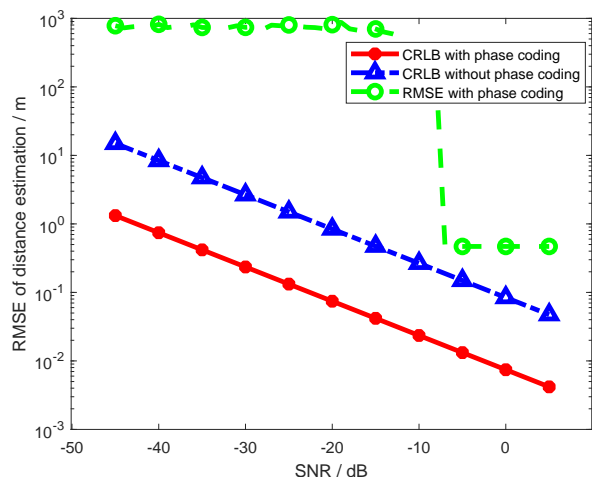


Fig. 12: Distance estimation performance of proposed ISAC signal.

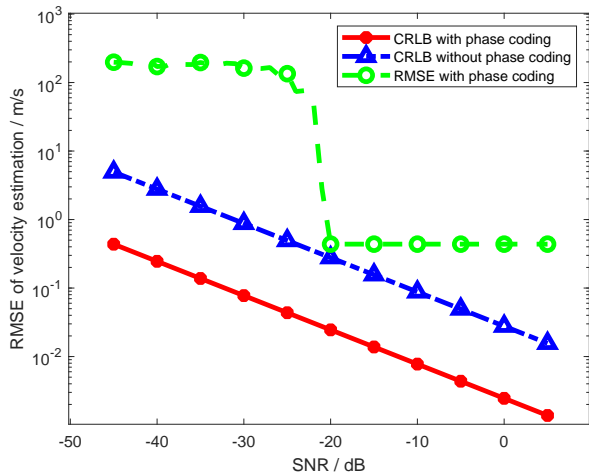


Fig. 13: Velocity estimation performance of proposed ISAC signal.

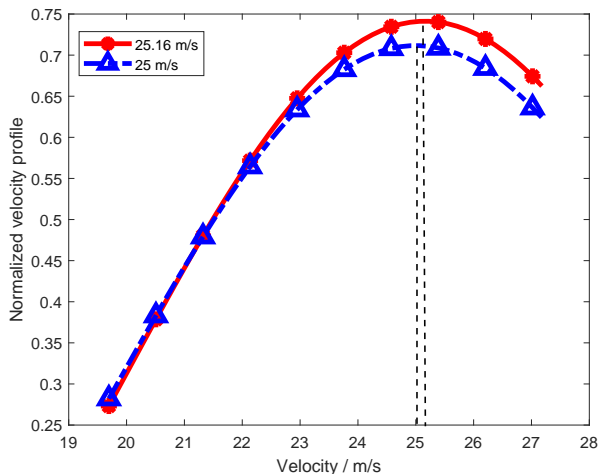


Fig. 14: Velocity estimation performance in long distance sensing.

targets, while the two targets can still be distinguished with the iterative CC algorithm.

VI. CONCLUSION

In this paper, in order to improve the anti-noise performance of ISAC signal, phase coding is applied in ISAC signal design combining the pilot and data signals. Then, the CRLB of the ISAC signal is analyzed. The iterative ISAC signal processing algorithms with high accuracy and low-complexity are proposed. Taking the short distance and long distance sensing scenarios into account, the iterative ISAC signal processing methods are proposed based on 2D FFT and CC algorithms, respectively. This paper provides the iterative ISAC signal processing algorithms with high accuracy and low complexity, which is promising to be applied in the energy efficient ISAC systems.

REFERENCES

- [1] "3GPP. TS 38.211 NR; Physical channels and modulation," 3rd Generation Partnership Project (3GPP), Technical Specification (TS) 38.211, 2021.
- [2] F. Liu, C. Masouros, A. P. Petropulu, H. Griffiths, and L. Hanzo, "Joint radar and communication design: Applications, state-of-the-art, and the road ahead," *IEEE Transactions on Communications*, vol. 68, no. 6, pp. 3834–3862, 2020.
- [3] W. Yuan, F. Liu, C. Masouros, J. Yuan, D. W. K. Ng, and N. Gonzalez-Prelcic, "Bayesian Predictive Beamforming for Vehicular Networks: A Low-Overhead Joint Radar-Communication Approach," *IEEE Transactions on Wireless Communications*, vol. 20, no. 3, pp. 1442–1456, 2021.
- [4] F. Liu, W. Yuan, C. Masouros, and J. Yuan, "Radar-Assisted Predictive Beamforming for Vehicular Links: Communication Served by Sensing," *IEEE Transactions on Wireless Communications*, vol. 19, no. 11, pp. 7704–7719, 2020.
- [5] Z. Feng, Z. Fang, Z. Wei, X. Chen, Z. Quan, and D. Ji, "Joint radar and communication: A survey," *China Communications*, vol. 17, no. 1, pp. 1–27, 2020.
- [6] "Introduction to 6G | IMT-2030." [Online]. Available: <https://www.tonex.com/training-courses/introduction-to-6g-imt-2030>. Apr. 2020.
- [7] J. A. Zhang, F. Liu, C. Masouros, R. W. Heath Jr, Z. Feng, L. Zheng, and A. Petropulu, "An Overview of Signal Processing Techniques for Joint Communication and Radar Sensing," *arXiv preprint arXiv:2102.12780*, 2021.
- [8] A. R. Chiriyath, B. Paul, and D. W. Bliss, "Radar-communications convergence: Coexistence, cooperation, and co-design," *IEEE Transactions on Cognitive Communications and Networking*, vol. 3, no. 1, pp. 1–12, 2017.
- [9] X. Chen, Z. Feng, Z. Wei, P. Zhang, and X. Yuan, "Code-division OFDM joint communication and sensing system for 6G machine-type communication," *IEEE Internet of Things Journal*, vol. 8, no. 15, pp. 12 093–12 105, 2021.
- [10] K. Chen, Y. Liu, and W. Zhang, "Study on integrated radar-communication signal of OFDM-LFM based on FRFT," 2015.
- [11] F. Uysal, "Phase-coded FMCW automotive radar: System design and interference mitigation," *IEEE Transactions on Vehicular Technology*, vol. 69, no. 1, pp. 270–281, 2019.
- [12] L. Hu, Z. Du, and G. Xue, "Radar-communication integration based on OFDM signal," in *2014 IEEE international conference on signal processing, communications and computing (ICSPCC)*. IEEE, 2014, pp. 442–445.
- [13] X. Tian, T. Zhang, Q. Zhang, and Z. Song, "Waveform design and processing in OFDM based radar-communication integrated systems," in *2017 IEEE/CIC International Conference on Communications in China (ICCC)*. IEEE, 2017, pp. 1–6.
- [14] X. Tian and Z. Song, "On radar and communication integrated system using OFDM signal," in *2017 IEEE Radar Conference (RadarConf)*. IEEE, 2017, pp. 0318–0323.
- [15] J. Zhao, K. Huo, and X. Li, "A chaos-based phase-coded OFDM signal for joint radar-communication systems," in *2014 12th international conference on signal processing (ICSP)*. IEEE, 2014, pp. 1997–2002.
- [16] L. Qi, Y. Yao, B. Huang, and G. Wu, "A Phase-coded OFDM Signal for Radar-communication Integration," in *2019 IEEE International Symposium on Phased Array System & Technology (PAST)*. IEEE, 2019, pp. 1–4.
- [17] R. F. Tigrek and P. Van Genderen, "A Golay code based approach to reduction of the PAPR and its consequence for the data throughput," in *2007 European Radar Conference*. IEEE, 2007, pp. 146–149.
- [18] W. Li, Z. Xiang, and P. Ren, "Waveform Design for Dual-Function Radar-Communication System With Golay Block Coding," *IEEE Access*, vol. 7, pp. 184 053–184 062, 2019.
- [19] C. Sturm and W. Wiesbeck, "Waveform design and signal processing aspects for fusion of wireless communications and radar sensing," *Proceedings of the IEEE*, vol. 99, no. 7, pp. 1236–1259, 2011.
- [20] K. Wu, J. A. Zhang, X. Huang, and Y. J. Guo, "Integrating Low-Complexity and Flexible Sensing into Communication Systems," *arXiv preprint arXiv:2109.04109*, 2021.
- [21] Y. Zeng, Y. Ma, and S. Sun, "Joint radar-communication with cyclic prefixed single carrier waveforms," *IEEE Transactions on Vehicular Technology*, vol. 69, no. 4, pp. 4069–4079, 2020.
- [22] J. Li, S. An, J. An, H. Zirath, and Z. S. He, "OFDM radar range accuracy enhancement using fractional Fourier transformation and phase analysis techniques," *IEEE Sensors Journal*, vol. 20, no. 2, pp. 1011–1018, 2019.

- [23] A. Tang, S. Li, and X. Wang, "Self-interference-resistant IEEE 802.11 ad-based joint communication and automotive radar design," *IEEE Journal of Selected Topics in Signal Processing*, vol. 15, no. 6, pp. 1484–1499, 2021.
- [24] R. Schmidt, "Multiple emitter location and signal parameter estimation," *IEEE transactions on antennas and propagation*, vol. 34, no. 3, pp. 276–280, 1986.
- [25] R. Roy, A. Paulraj, and T. Kailath, "ESPRIT—A subspace rotation approach to estimation of parameters of cisoids in noise," *IEEE transactions on acoustics, speech, and signal processing*, vol. 34, no. 5, pp. 1340–1342, 1986.
- [26] U. Tureli, H. Liu, and M. D. Zoltowski, "OFDM blind carrier offset estimation: ESPRIT," *IEEE Transactions on communications*, vol. 48, no. 9, pp. 1459–1461, 2000.
- [27] K. Wu, J. A. Zhang, X. Huang, and Y. J. Guo, "OTFS-based joint communication and sensing for future industrial IoT," *IEEE Internet of Things Journal*, 2021.
- [28] F. Uysal, "Phase-coded FMCW automotive radar: System design and interference mitigation," *IEEE Transactions on Vehicular Technology*, vol. 69, no. 1, pp. 270–281, 2019.